Atmos. Chem. Phys. Discuss., 14, 19515–19544, 2014
www.atmos-chem-phys-discuss.net/14/19515/2014/
doi:10.5194/acpd-14-19515-2014

Atmospheric Chemistry and Physics Discussions

Constraints on Asian ozone using Aura TES, OMI and Terra MOPITT

Z. Jiang[1], J. R. Worden[1], D. B. A. Jones[2,3], J. T. Lin[4], W. W. Verstraeten[5,6], and D. K. Henze[7]

[1]Jet Propulsion Laboratory, California Institute of Technology, Pasadena, CA, USA
[2]Department of Physics, University of Toronto, Toronto, ON, Canada
[3]JIFRESSE, University of California, Los Angeles, Los Angeles, CA, USA
[4]Laboratory for Climate and Ocean–Atmosphere Studies, Department of Atmospheric and Oceanic Sciences, School of Physics, Peking University, Beijing, China
[5]Meteorology and Air Quality Department, Wageningen University, the Netherlands
[6]Earth Observation Climate Department, Royal Netherlands Meteorological Institute, the Netherlands
[7]Department of Mechanical Engineering, University of Colorado, Boulder, CO, USA

Received: 25 June 2014 – Accepted: 17 July 2014 – Published: 29 July 2014

Correspondence to: Z. Jiang (zhe.jiang@jpl.nasa.gov)

Published by Copernicus Publications on behalf of the European Geosciences Union.

Abstract

Rapid industrialization in Asia in the last two decades has resulted in a significant increase in Asian ozone (O_3) pre-cursor emissions with likely a corresponding increase in the export of O_3 and its pre-cursors. However, the relationship between this increasing O_3, the chemical environment, O_3 production efficiency, and the partitioning between anthropogenic and natural precursors is unclear. In this work, we use satellite measurements of O_3, CO and NO_2 from TES (Tropospheric Emission Spectrometer), MOPITT (Measurement of Pollution In The Troposphere) and OMI (Ozone Monitoring Instrument) to quantify O_3 pre-cursor emissions for 2006 and their impact on free-tropospheric O_3 over North-East Asia, where pollution is typically exported globally due to strong westerlies. Using the GEOS-Chem global chemical transport model, we show that the modeled seasonal variation of O_3 based on these updated O_3 pre-cursor emissions is consistent with the observed O_3 variability and amount, after accounting for known biases in the TES O_3 data. Using the adjoint of GEOS-Chem we then partition the relative contributions of natural and anthropogenic sources to free troposphere O_3 in this region. We find that the influence of lightning NO_x is important in summer. The contribution from anthropogenic NO_x is dominant in other seasons. China is the major contributor of anthropogenic VOCs (Volatile Organic Compounds), whereas the influence of biogenic VOCs is mainly from Southeast Asia. Our result shows that the influence of India and Southeast Asia emissions on O_3 pollution export is significant, comparable with Chinese emisisons in winter and about 50 % of Chinese emissions in other seasons.

1 Introduction

Unprecedented growth in transportation, coal-fired power plants and the industrial sector in China has resulted in a substantial increase in the emissions of O_3 precursors (Lin et al., 2014a). Recent studies (Lamsal et al., 2011; Lin, 2012; Mijling et al., 2013)

ACPD
14, 19515–19544, 2014

show 5–10 % annual growth rate of NO_x emission in China. Wang et al. (2012) found there is 3 % annual growth rate of O_3 in Beijing in the period of 2003–2010. East Asian O_3 can be transported to the surface of North America in about 2–3 weeks (Liu and Mauzerall, 2005) by midlatitude westerly winds (Liang et al., 2004, 2005), which likely results in an increase of background O_3 concentration in western North America by 3–7 ppbv (Zhang et al., 2008; Brown et al., 2011).

Use of inverse (top-down) methods to better quantify the emission of NO_x (Lamsal et al., 2011; Lin and McElroy, 2011; Lin, 2012; Mijling et al., 2013), VOCs (Shim et al., 2005; Fu et al., 2007) and CO (Kopacz et al., 2010; Fortems-Cheiney et al., 2011; Gonzi et al., 2011) are needed to ensure consistency between bottom-up inventories and observations. However, large discrepancies can still exist between bottom-up and top-down based inventories (e.g., Kopacz et al., 2010; Lin et al., 2012b). In this work, we perform a multi-tracer assimilation with the GEOS-Chem model to evaluate the top-down estimates of O_3 precursors (NO_x and CO) in East Asia. We firstly optimized the CO and NO_x emission with MOPITT CO and OMI NO_2 retrievals respectively and then evaluate the a posteriori simulation of CO and O_3 by comparing the values with measurements from TES in June–August 2006. Using the adjoint of the GEOS-Chem model (Henze et al., 2007), we then quantify source contributions (NO_x, CO, VOC) to free tropospheric O_3 pollution over East China and the China outflow region in December 2005–November 2006.

2 Observations and model

2.1 TES CO and O_3

The TES instrument was launched on NASA's Aura spacecraft on 15 July 2004. The satellite is in a sun-synchronous polar orbit of 705 km and crosses the equator at 01:45 and 13:45 LT. With a footprint of 8 km × 5 km, TES measures radiances between 3.3–15.4 µm with global coverage of 16 days (Beer et al., 2001) of observations. In the

ACPD
14, 19515–19544, 2014

troposphere, TES O_3 profile retrievals have 1–2 degrees of freedom for signal (DOFS), and about 1 DOFS for CO. We use data from the "lite" product (http://tes.jpl.nasa.gov/data/) which reports volume mixing ratios (VMR) on 26 pressure levels for O_3 and 14 pressure levels for CO. Using an optimal estimation approach, the TES retrievals are conducted with respect to the logarithm of the VMR. The relationship between the retrieved profiles and the true atmospheric state can be expressed as:

$$\hat{z}^{\mathrm{TES}} = z_{\mathrm{a}}^{\mathrm{TES}} + \mathbf{A}^{\mathrm{TES}}\left(z - z_{\mathrm{a}}^{\mathrm{TES}}\right) + \mathbf{G}\varepsilon \quad (1)$$

where z is the true atmospheric state (expressed as log(VMR)), $z_{\mathrm{a}}^{\mathrm{TES}}$ is the TES a priori O_3 or CO profile, $\mathbf{A}^{\mathrm{TES}}$ is the TES averaging kernel matrix and $\mathbf{G}\varepsilon$ describes the retrieval error. The averaging kernel matrix represents the sensitivity of the retrieval to the actual trace gas in the atmosphere. The TES retrievals use a monthly mean profile of the trace gas from the MOZART-4 CTM (chemical transport model), averaged over a 10° latitude ×60° longitude, as the a priori information $z_{\mathrm{a}}^{\mathrm{TES}}$. According to the recommended quality control criterion, we only use CO and O_3 data with major quality flag equals 1. The data with small DOFS (Degree of Freedom for Signal for CO is smaller than 0.8), are dropped as the limited sensitivity reduces the robustness of the calculated O_3-CO correlations.

2.2 MOPITT CO

The MOPITT instrument was launched on NASA's Terra spacecraft on 18 December 1999. The satellite is in a sun-synchronous polar orbit of 705 km and crosses the equator at 10:30 LT. With a footprint of 22 km × 22 km, MOPITT (version 6) combines TIR (4.7 µm) with the NIR (2.3 µm) and has better sensitivity to lower tropospheric CO over land (Worden et al., 2010). MOPITT CO retrievals are reported on 10 pressure levels (surface, 900, 800, 700, 600, 500, 400, 300, 200 and 100 hPa). Similar to the TES product, relationship between the retrieved CO profiles and the true atmospheric

ACPD
14, 19515–19544, 2014

state can be expressed as:

$$\hat{z}^{\mathrm{MOP}} = z_{\mathrm{a}}^{\mathrm{MOP}} + \mathbf{A}^{\mathrm{MOP}}\left(z - z_{\mathrm{a}}^{\mathrm{MOP}}\right) + \mathbf{G}\varepsilon \quad (2)$$

where z is the true atmospheric state (expressed as log(VMR)), $z_{\mathrm{a}}^{\mathrm{MOP}}$ is the MOPITT a priori CO profile, $\mathbf{A}^{\mathrm{MOP}}$ is the MOPITT averaging kernel matrix and $\mathbf{G}\varepsilon$ describes the retrieval error.

The MOPITT retrievals use a monthly mean profile from the MOZART-4 CTM as the a priori information. We reject MOPITT data with CO column amounts less than 5×10^{17} molec cm^{-2} and if low clouds are observed. The nighttime data is excluded in the assimilation, due to the NIR radiances measure reflected solar radiation. The version 5 data have been evaluated recently against NOAA aircraft measurements (Deeter et al., 2013), which shows small bias in the low and middle troposphere, but 14 % positive bias at 200 hPa retrieval level. The new version 6 data significantly reduces the bias in the upper troposphere but magnifies the positive bias at the surface level. In this work, we decide to use the new version 6 data, as we focus on the free troposphere, which is not affected by the positive bias in the retrieval at the surface level.

2.3 OMI NO_2

The OMI instrument was also launched on NASA's Aura spacecraft. The sensor has a spatial resolution of 13 km × 24 km (Levelt et al., 2006). OMI provides daily global coverage with measurements of both direct and atmosphere-backscattered sunlight in the ultraviolet-visible range from 270 to 500 nm; 405–465 nm is used to retrieve tropospheric NO_2 columns. In this study, the daily level-2 data from KNMI DOMINO-2 product (Boersma et al., 2011) are averaged to obtain monthly mean vertical column densities (VCDs) for subsequent emission inversion. The details for the data treatment are described in Lin (2012).

ACPD
14, 19515–19544, 2014

2.4 GEOS-Chem

The GEOS-Chem CTM (http://www.geos-chem.org) is driven by assimilated meteorological observation from the NASA Goddard Earth Observing System (GEOS-5) at the Global Modeling and data Assimilation Office. We use version v34 of the GEOS-Chem adjoint, which is based on v8-02-01 of GEOS-Chem, with relevant updates through v9-01-01. The standard GEOS-Chem chemistry mechanism includes 43 tracers, which can simulate detailed tropospheric O_3–NO_x–hydrocarbon chemistry, including the radiative and heterogeneous effects of aerosols. The GEOS-5 meteorological fields have 72 vertical levels and the lowest 31 levels are terrain following levels. In order to minimize the amount of memory required to run GEOS-Chem, the model is run with a reduced vertical resolution, in which the levels in the stratosphere are lumped together online.

The native horizontal resolution of GEOS-5 is $0.5^\circ \times 0.667^\circ$, but it is usually degraded to $4^\circ \times 5^\circ$ or $2^\circ \times 2.5^\circ$ in global scale simulations. A nested simulation can be achieved by running a $0.5^\circ \times 0.667^\circ$ resolution model within a regional domain using the boundary condition provided from a global, coarse resolution mode (Wang et al., 2004; Chen et al., 2009). Recently, the adjoint of nested GEOS-Chem was developed by Jiang et al. (2014). In this work, following Jiang et al. (2014), we run the model with $0.5^\circ \times 0.667^\circ$ resolution over Asia. The boundary condition is generated with a global-scale $4^\circ \times 5^\circ$ resolution simulation.

The anthropogenic emission inventories are identical to those used in Jiang et al. (2013). The global anthropogenic emission inventory is EDGAR 3.2FT2000 (Olivier et al., 2001), updated by the following regional emission inventories: the INTEX-B Asia emissions inventory for 2006 (Zhang et al., 2009b), the Cooperative Program for Monitoring and Evaluation of the Long-range Transmission of Air Pollutants in Europe (EMEP) inventory for Europe in 2000 (Vestreng et al., 2002), the US Environmental Protection Agency National Emission Inventory (NEI) for 2005 in North America, the Criteria Air Contaminants (CAC) inventory for Canada, and the Big Bend Regional

ACPD
14, 19515–19544, 2014

Aerosol and Visibility Observational (BRAVO) Study Emissions Inventory for Mexico (Kuhns et al., 2003). Biomass burning emissions are from the inter-annual GFED3 inventory with 3 h resolution (van der Werf et al., 2010). The biogenic emissions are from MEGAN 2.0 (Millet et al., 2008). Figure 1 shows the anthropogenic emission of NO_x and CO in Asia in June 2006. There are strong pollutant emissions in the North China Plain. The urban emission centers can also be clearly identified.

3 Inversion approach

3.1 4DVAR inversion for global CO emission

The 2006 global CO emissions are optimized with a 4DVAR method. The inverse method minimizes the cost function $J(\boldsymbol{x})$ to provide an optimal estimate of the CO sources,

$$J(\boldsymbol{x}) = (\mathbf{F}(\boldsymbol{x}) - \boldsymbol{y})^{\mathrm{T}}\mathbf{S}_{\Sigma}^{-1}(\mathbf{F}(\boldsymbol{x}) - \boldsymbol{y}) + (\boldsymbol{x} - \boldsymbol{x}_{\mathrm{a}})^{\mathrm{T}}\mathbf{S}_{\mathrm{a}}^{-1}(\boldsymbol{x} - \boldsymbol{x}_{\mathrm{a}}) \quad (3)$$

where $\boldsymbol{x}$ is the state vector of emissions, $\boldsymbol{x}_{\mathrm{a}}$ is the a priori estimate, $\boldsymbol{y}$ is a vector of observed concentrations, and $\mathbf{F}(\boldsymbol{x})$ is the forward model, which represents the transport of the CO emissions in the GEOS-Chem model and accounts for the vertical smoothing of the MOPITT retrieval. $\mathbf{S}_{\Sigma}$ and $\mathbf{S}_{\mathrm{a}}$ are the observational and a priori error covariance matrices, respectively. The first term of the cost function represents the mismatch between the simulated and observed concentrations. The second term represents the departure of the estimate from the a priori.

The cost function in Eq. (3) is minimized by reducing the gradient, $\partial J/\partial x$, using the adjoint of GEOS-Chem model in a 4DVAR approach (Henze et al., 2007), which has been previously used for assimilation of CO and O_3 (Kopacz et al., 2010; Singh et al., 2011; Parrington et al., 2012; Jiang et al., 2014b). Similar as in Jiang et al. (2013, 2014b), we produce improved initial conditions by assimilating MOPITT version 6 data,

ACPD
14, 19515–19544, 2014

using the sequential sub-optimal Kalman filter (Parrington et al., 2008), from 1 January 2006 to 1 January 2007. The optimized initial conditions are archived at the beginning of each month. Consequently, the initial conditions for the model simulation are independent from the inverse analyses.

3.2 Regression-based inversion for China NO_x emissions

The 2006 Chinese NO_x emissions are optimized with a regression-based multi-step method exploiting the distinctive seasonality of different sources (Lin, 2012). Neglecting horizontal transport and assuming a linear relationship between the total VCD of NO_2 and VCDs from individual sources, the predicted VCD (Ω_p) for a given grid can be expressed as the sum of individual emission sources, multiplied by certain scaling factors:

$$\Omega_p = k_a\Omega_a + k_l\Omega_l + k_s\Omega_s + k_b\Omega_b \quad (4)$$

The subscripts "a", "l", "s", and "b" indicate anthropogenic, lightning, soil and biomass burning sources of NO_x, respectively. The updated emission estimates can be obtained by reducing the sum of $[(\Omega_r - \Omega_p)/\sigma]^2$ across the 12 months; here Ω_r is the retrieved VCD and σ is the standard deviation. To better represent the resolution-dependent NO_x chemistry (Valin et al., 2011), the inversion was conducted with the highest resolution of GEOS-Chem. The seasonality-based inversion method also reduced the influence of potential biases in OMI NO_2 data (Lin et al., 2014b), particularly in winter. The details for the inversion process were described in Lin (2012).

ACPD
14, 19515–19544, 2014

4 Results and discussion

4.1 Evaluation of the model simulation and top-down estimates of O_3 precursors

In this work, we are interested in the domain of East China, as shown in Fig. 1, because it is the largest pollutant emission contributor in East Asia. We will also study the domain where outflow of Asian pollution dominates. Figure 2 shows the monthly regional mean O_3 and CO concentration at 681 hPa for June, July and August for the period 2006–2010, driven with a priori emission inventories. The modeled O_3 concentrations are generally within 10 % of the TES data after accounting for the approximately 7 ppb bias in the TES O_3 measurements (e.g., Worden et al., 2007; Verstraeten et al., 2013). On the other hand, the modeled CO is biased low. This could be associated with the positive bias in OH, as indicated by Jiang et al. (2014b). The bias can be reduced by integrating the coarse-resolution global and fine-resolution nested simulations in a two-way coupled manner, such that results from the nested model can be used to improve the global model (within the nested domain) and ultimately affect its lateral boundary conditions (via the global transport of CO and other species) (Yan et al., 2014). Another possible reason is that the TES CO data are biased towards polluted air parcels because of its relatively low sensitivity whereas the model captures background values as discussed in Pechony et al. (2013). Both model and TES show similar trends and interannual variability indicating that changes in the modeled emissions and their chemical production of ozone are well described with the changes in the bottom up emissions.

O_3–CO correlations can be used to constrain O_3 sources and transport (e.g., Zhang et al., 2006). Positive correlations usually indicate that a region has experienced photochemical O_3 production, whereas negative correlations may result from O_3 chemical loss or influence of stratospheric air. For example, Zhang et al. (2006) demonstrated that TES data can be used to examine global distribution of O_3–CO correlations. Voulgarakis et al. (2011) found significant positive correlations in the northern Pacific during the summer of 2005–2008. Kim et al. (2013) used OMI O_3 and AIRS CO to show that

ACPD
14, 19515–19544, 2014

the GEOS-Chem model is able to reproduce the observed O_3–CO correlations and slopes in western Pacific, but failed in some tropical regions due to model transport error associated with deep convection.

Table 1 shows the monthly regional mean O_3 and CO correlation and slope values for the free troposphere (825–383 hPa) for June, July and August 2006–2010; the model is driven by a priori emissions. The uncertainty in the O_3 and CO concentrations are due to random errors in the TES O_3 and CO observations and natural variability (Zhang et al., 2006). For this reason, we also show the mean value over the analysis time period. The correlation and slope values of TES and GEOS-Chem are generally consistent for both domains. The positive correlation coefficients imply influence of photochemical O_3 production, which become stronger from continent to the ocean outflow domains. As in previous studies (Zhang et al., 2006; Voulgarakis et al., 2011; Kim et al., 2013), there are small difference between the simulation and observation. There are relatively large discrepancies over the ocean, perhaps due to transport error because transport of "clean" air from the Pacific can have substantially different chemical characteristics from Asian air.

The consistency between model and TES in the interannual varations, correlation coefficients and slopes demonstrates that the model has good agreement with data over East Asia and Northwest Pacific (or Asian outflow region). The next step is an evaluation of the uncertainties in the emission inventories. As described in Sect. 3, the 2006 global CO emission are constrained with MOPITT data; the 2006 Chinese NO_x emission are constrained with OMI data. As shown in Fig. 3, Chinese anthropogenic NO_x emission in June 2006 is enhanced by 14 %, from 1.86 Tg to 2.11 Tg. Similar adjustment is obtained for winter with smaller magnitude. In June 2006, the Chinese anthropogenic CO emission is increased from 17.09 Tg to 18.93 Tg, with a mean scaling factor of 1.11. The small uncertainty in the CO emission in summer is consistent with Jiang et al. (2014b).

The monthly regional mean O_3 and CO concentrations of the a posteriori simulation for June, July and August 2006 are shown in Fig. 2. In order to remove the influence

ACPD
14, 19515–19544, 2014

of the initial conditions, the updated-simulation is obtained by running the model from 1 January 2006, with updated inventories of NO_x and CO. Over the China outflow region, the updated simulation reduces the bias relative to TES by 30 % for CO and 20 % for O_3. Over eastern China, the bias relative to TES is reduced by 40 % for CO. It is not surprising to see the updated inventories had only a modest impact for O_3 since the agreement between the a priori and the observation was already good (to within 10 % in June and better than 1 % in July and August). The significant reduction in the relative bias provides confidence that the chemical scheme is sufficient to evaluate the partitioning of the natural and anthropogenic emissions.

Because the updated NO_x and CO emissions are only slightly higher (about 10 %) than the a priori, the response of O_3 to this discrepancy should be linear, as indicated by Wild et al. (2012). To avoid the influence of potential bias in the top-down emission estimations (Jiang et al., 2011; Lin et al., 2012b), it will be good to use the a priori emission inventories in the following analysis. Its effect on the partition, based on the monthly/seasonal regional mean free tropospheric O_3, should be ignorable.

4.2 Dependency of O_3 on anthropogenic and natural NO_x, CO and VOCs

In this section, we will use the adjoint of the GEOS-Chem model (Henze et al., 2007) to quantify source contributions (NO_x, CO, VOC) to free tropospheric O_3 pollution over East China and the China Outflow region. We are interested in these two domains as they have significant influence on the long-range pollution transport. Similar to previous studies (Zhang et al., 2009; Bowman et al., 2012; Lapina et al., 2014), the analysis is based on a sensitivity calculation from an adjoint model. In this work, both transport and chemistry components are run backwards and thus provide a more computationally efficient method for a receptor-oriented problem than the traditional approach by perturbing emissions.

Figure 4 shows the contributions of anthropogenic NO_x, lightning NO_x, anthropogenic CO and biogenic isoprene on free tropospheric (819–396 hPa) O_3 over eastern China. The value can be explained as the percentage change of regional mean

ACPD
14, 19515–19544, 2014

O_3 due to a fractional change in emissions in a particular grid. For example, assuming unchanged chemical environment, one particular grid with contribution 0.02 % implies mean free tropospheric O_3 over eastern China will be increased by 0.02 %, if the NO_x emission in this gird is increased by 100 %. The result shows that anthropogenic NO_x contributes significantly to the O_3 distribution in this region. Although the influence of lightning NO_x is weaker, the larger geographical distribution of lightning NO_x makes it an important source. The contribution of anthropogenic CO is mainly from China, whereas Southeast Asia is the major contributor of biogenic isoprene with a negative sensitivity. It implies China is the major source of anthropogenic hydrocarbons and Southeast Asia is the major source of biogenic hydrocarbons. It should be reminded that the sensitivity to biogenic isoprene is highly dependent on the isoprene chemistry scheme, as indicated by Mao et al. (2013). The contributions on the China Outflow region free troposphere O_3 are shown in Fig. 5. The O_3 distribution is more sensitive to the anthropogenic NO_x emission from the coast rather than from the inland continent. The sensitivity hotspots clearly show a northeastward movement as the season progresses, from Southeast China (June) to Korean and Japan (August), reflecting the influence of the East Asia monsoon.

To understand the seasonal variation of O_3 production efficiency, we calculated the global scale sensitivities of anthropogenic and lightning NO_x during December 2005–November 2006 with $4^\circ \times 5^\circ$ resolution. The values of sensitivities, as shown in Fig. 6, are significantly larger than those in Figs. 4 and 5, due to the change of grid size and smaller effect from initial condition, which will be discussed later. The sensitivity of O_3 to anthropogenic NO_x, has a marked seasonal variation, increasing from the Northern Hemisphere winter to the summer. Kondo et al. (2008) found the slope of East Asia O_3 formation to NO_x is proportional to HO_2 and thus increases from winter to spring. Increased solar radiation is another reason for the high O_3 production rate in the summer. Figure 6 also highlights the effect of anthropogenic NO_x from southwest China, showing a significant effect on free troposphere O_3 over eastern China, particularly in September–November. Similar to anthropogenic NO_x, the contribution of lightning NO_x

ACPD
14, 19515–19544, 2014

is maximum in the Northern Hemisphere summer, partly associated with the East Asia monsoon. The sensitivities of O_3 over eastern China and the China Outflow region have similar distributions, although the China Outflow O_3 is more sensitive to coastal emissions.

Table 2 shows the regional total contributions of anthropogenic and lightning NO_x, calculated by summing the sensitivities shown in Fig. 6. Assuming unchanged chemical environment, it can be explained as the percentage change of regional mean O_3 due to 100 % change in NO_x emission with current O_3 production efficiency. For example, 100 % increase of Chinese anthropogenic NO_x emission in June–August 2006 will result in 10.16 % increase of tropospheric mean O_3 over eastern China. Of course, the result of an actual 100 % change of NO_x will be different to quantify because of non-linear chemistry. Furthermore, this sensitivity depends on the modeled transport and the robustness of the chemical production of ozone. For example, if the production of ozone is too "fast" then the sensitivity of free-tropospheric ozone to surface emissions is too small as too much ozone is produced in the boundary layer (where loss-mechanisms dominate) vs. the free-troposphere. To evaluate the sensitivities further, we enhanced Chinese anthropogenic NO_x emission by 10 % uniformly as a perturbation. Using the initial conditions provided from standard simulation, the 3 month perturbation simulations are started on 1 December 2005, 1 March 2006, 1 June 2006 and 1 September 2006, individually. The relative difference of regional mean O_3, between the perturbation and standard simulations, is then multiplied by 10. As shown in Table 2, the results of two methods are highly consistent, which demonstrates our sensitivity analysis works well. Similar as Wild et al. (2012), the consistency also confirms that 10 % NO_x perturbation gives linear O_3 responses over East Asia. Considering the high computation efficiency, adjoint sensitivity analysis is thus a good alternative to the traditional perturbation method.

As shown in Table 2, the effect of increased Chinese anthropogenic NO_x on free troposphere O_3 is limited. Assuming an unchanged chemical environment, a 100 % increase of Chinese anthropogenic NO_x, during a 3 month period, will only result in

ACPD
14, 19515–19544, 2014

2.68 % increase of free tropospheric O_3 in the winter and 10.16 % in the summer, associated with the chemical environment of China, which is is more inclined to be VOC limited. Furthermore, O_3 distribution in initial conditions are not affected by the change of NO_x emission. Because of the long O_3 lifetime in the free troposphere, O_3 from initial conditions have a substantial influence on the distribution of ozone. A 18 month continous perturbation simulation, started on 1 June 2005, will enhance the effect of Chinese anthropogenic NO_x to 3.27 % in winter and 10.46 % in summer.

Over eastern China, the effect of anthrogogenic NO_x emission from the ROA on free tropospheric O_3 is about 50 % of Chinese local emission in winter and spring, whereas Chinese local emission dominates in the summer and fall. The large contribution of ROA is mainly due to the fact that free tropospheric (819–396 hPa) O_3 values are used in this analysis. According to our test, the boundary layer (surface–819 hPa) O_3 is highly dependent on China local emission rather than long-range transport.

Because of the rapid growth of pollutant emission, transpacific transport of Asian pollutant to North America has attractted significant attention (Zhang et al., 2008, 2009; Walker et al., 2010; Bertram et al., 2013; Lin et al., 2008, 2014a). The major transport mechanisms includes northeastward export of Asian pollution to about 50° N, and then cross the Pacific in midlatitude westerly winds (Liang et al., 2004, 2005). Our results show that the influence of ROA on O_3 pollution export is significant. In the China Outflow region, the influence of ROA is comparable with Chinese emisisons in winter and about 50 % of Chinese emissions in other seasons. The contribution of lightning NO_x over China is generally small relative to anthropogenic emisisons except during the summer (Table 2). The effect of ROA lightning NO_x is similar as the Chinese contribution but slightly larger.

5 Summary

We quantified Asian O_3 and the contributions of its precursors, during the period December 2005–November 2006, using the GEOS-Chem model and O_3 precursor

ACPD
14, 19515–19544, 2014

observations of NO_2 from OMI and CO from MOPITT. The 2006 global CO emissions are constrained with a 4DVAR method, using MOPITT CO (version 6) measurements. In June 2006, the inversion increases the China anthropogenic CO emission by 11 %. The 2006 China NO_x emission is constrained with a regression-based multi-step approach, using OMI data. In June 2006, the anthropogenic NO_x emission in China is increased by 14 %.

The model simulation was evaluated with TES O_3 and CO observations. The modeled concentrations are underestimated for both O_3 and CO, but reproduces the O_3 (CO) interannual varation quite well. As with previous studies (Zhang et al., 2006; Voulgarakis et al., 2011; Kim et al., 2013), the modeled O_3–CO correlation and slope are consistent with the data. The updated inventories reduces the bias relative to TES measurements. Over the China Outlfow region, it is reduced by 20 % for O_3 and 30 % for CO. The good agreement between model O_3 and CO and its correlations with observations from TES demonstrate the reliability of the model simulation, the chemical scheme and the updated inventories.

We quantified source contributions (NO_x, CO, VOC) to free tropospheric O_3 pollution over East China and the China Outflow region with a sensitivity calculation approach. Our results show anthropogenic emissions from the Rest-of-Asia (ROA) has an important influence on free tropospheric O_3 over China and its outflow region and consequently background O_3 concentrations of North America. The observed seasonal variation in O_3 is due to the seasonal change in the O_3 production efficiency, related with HO_2 and solar radiation. The contributions of lightning NO_x to free-tropospheric O_3 from China and ROA is small, except in June–August due to the effect of the East Asia monsoon. Finally, our result shows that China is the major contributor of anthropogenic VOCs, whereas the influence of biogenic VOCs is mainly from Southeast Asia.

Acknowledgements. Part of this research was carried out at the Jet Propulsion Laboratory, California Institute of Technology, under a contract with the National Aeronautics and Space Administration. This Research was supported by the NASA ROSES Aura Science Team NNH10ZDA001N-AURA. Daven K. Henze was funded by NASA ACMAP NNX13AK86G.

ACPD
14, 19515–19544, 2014

Willem W. Verstraeten was funded by the Netherlands Organization for Scientific Research, NWO Vidi grant 864.09.001.

References

Beer, R., Glavich, T. A., and Rider, D. M.: Tropospheric emission spectrometer for the Earth Observing System's Aura satellite, Appl. Optics, 40, 2356–2367, 2001.

Bertram, T. H., Perring, A. E., Wooldridge, P. J., Dibb, J., Avery, M. A., and Cohen, R. C.: On the export of reactive nitrogen from Asia: NO_x partitioning and effects on ozone, Atmos. Chem. Phys., 13, 4617–4630, doi:10.5194/acp-13-4617-2013, 2013.

Boersma, K. F., Eskes, H. J., Dirksen, R. J., van der A, R. J., Veefkind, J. P., Stammes, P., Huijnen, V., Kleipool, Q. L., Sneep, M., Claas, J., Leitão, J., Richter, A., Zhou, Y., and Brunner, D.: An improved tropospheric NO_2 column retrieval algorithm for the Ozone Monitoring Instrument, Atmos. Meas. Tech., 4, 1905–1928, doi:10.5194/amt-4-1905-2011, 2011.

Bowman, K. and Henze, D. K.: Attribution of direct ozone radiative forcing to spatially resolved emissions, Geophys. Res. Lett., 39, L22704, doi:10.1029/2012GL053274, 2012.

Brown-Steiner, B. and Hess, P.: Asian influence on surface ozone in the United States: a comparison of chemistry, seasonality, and transport mechanisms, J. Geophys. Res., 116, D17309, 2011.

Chen, D., Wang, Y., McElroy, M. B., He, K., Yantosca, R. M., and Le Sager, P.: Regional CO pollution and export in China simulated by the high-resolution nested-grid GEOS-Chem model, Atmos. Chem. Phys., 9, 3825–3839, doi:10.5194/acp-9-3825-2009, 2009.

Deeter, M. N., Martínez-Alonso, S., Edwards, D. P., Emmons, L. K., Gille, J. C., Worden, H. M., Pittman, J. V., Daube, B. C., and Wofsy, S. C.: Validation of MOPITT Version 5 thermal-infrared, near-infrared, and multispectral carbon monoxide profile retrievals for 2000–2011, J. Geophys. Res.-Atmos., 118, 6710–6725, 2013.

Fortems-Cheiney, A., Chevallier, F., Pison, I., Bousquet, P., Szopa, S., Deeter, M. N., and Clerbaux, C.: Ten years of CO emissions as seen from Measurements of Pollution in the Troposphere (MOPITT), J. Geophys. Res., 116, D05304, doi:10.1029/2010JD014416, 2011.

Fu, T.-M., Jacob, D. J., Palmer, P. I., Chance, K., Wang, Y. X., Barletta, B., Blake, D. R., Stanton, J. C., and Pilling, M. J.: Space-based formaldehyde measurements as constraints on

ACPD
14, 19515–19544, 2014

volatile organic compound emissions in east and south Asia and implications for ozone, J. Geophys. Res., 112, D06312, doi:10.1029/2006JD007853, 2007.
Gonzi, S., Feng, L., and Palmer, P. I.: Seasonal cycle of emissions of CO inferred from MOPITT profiles of CO: sensitivity to pyroconvection and profile retrieval assumptions, Geophys. Res. Lett., 38, L08813, doi:10.1029/2011GL046789, 2011.
Henze, D. K., Hakami, A., and Seinfeld, J. H.: Development of the adjoint of GEOS-Chem, Atmos. Chem. Phys., 7, 2413–2433, doi:10.5194/acp-7-2413-2007, 2007.
Jiang, Z., Jones, D. B. A., Kopacz, M., Liu, J., Henze, D. K., and Heald, C.: Quantifying the impact of model errors on top-down estimates of carbon monoxide emissions using satellite observations, J. Geophys. Res., 116, D15306, doi:10.1029/2010JD015282, 2011.
Jiang, Z., Jones, D. B. A., Worden, H. M., Deeter, M. N., Henze, D. K., Worden, J., Bowman, K. W., Brenninkmeijer, C. A. M., and Schuck, T. J.: Impact of model errors in convective transport on CO source estimates inferred from MOPITT CO retrievals, J. Geophys. Res.-Atmos., 118, 2073–2083, 2013.
Jiang, Z., Jones, D. B. A., Henze, D., Worden, H., and Wang, Y. X.: Regional data assimilation of multi-spectral MOPITT observations of CO over North America, Atmos. Chem. Phys., in preparation, 2014a.
Jiang, Z., Jones, D. B. A., Henze, D., and Worden, H.: Sensitivity of inferred regional CO source estimates to the vertical structure in CO as observed by MOPITT, Atmos. Chem. Phys., in preparation, 2014b.
Jones, D. B. A., Bowman, K. W., Logan, J. A., Heald, C. L., Liu, J., Luo, M., Worden, J., and Drummond, J.: The zonal structure of tropical O_3 and CO as observed by the Tropospheric Emission Spectrometer in November 2004 – Part 1: Inverse modeling of CO emissions, Atmos. Chem. Phys., 9, 3547–3562, doi:10.5194/acp-9-3547-2009, 2009.
Kim, P. S., Jacob, D. J., Liu, X., Warner, J. X., Yang, K., Chance, K., Thouret, V., and Nedelec, P.: Global ozone–CO correlations from OMI and AIRS: constraints on tropospheric ozone sources, Atmos. Chem. Phys., 13, 9321–9335, doi:10.5194/acp-13-9321-2013, 2013.
Kondo, J., Hudman, R. C., Nakamura, K., Koike, M., Chen, G., Miyazaki, Y., Takegawa, N., Blake, D. R., Simpson, I. J., Ko, M., Kita, K., and Shirai, T.: Mechanisms that influence the formation of high-ozone regions in the boundary layer downwind of the Asian continent in winter and spring, J. Geophys. Res., 113, D15304, doi:10.1029/2007JD008978, 2008.
Kopacz, M., Jacob, D. J., Fisher, J. A., Logan, J. A., Zhang, L., Megretskaia, I. A., Yantosca, R. M., Singh, K., Henze, D. K., Burrows, J. P., Buchwitz, M., Khlystova, I.,

ACPD
14, 19515–19544, 2014

McMillan, W. W., Gille, J. C., Edwards, D. P., Eldering, A., Thouret, V., and Nedelec, P.: Global estimates of CO sources with high resolution by adjoint inversion of multiple satellite datasets (MOPITT, AIRS, SCIAMACHY, TES), Atmos. Chem. Phys., 10, 855–876, doi:10.5194/acp-10-855-2010, 2010.

Kuhns, H., Green, M., and Etyemezian, V.: Big Bend Regional Aerosol and Visibility Observational (BRAVO) Study Emissions Inventory, Report prepared for BRAVO Steering Committee, Desert Research Institute, Las Vegas, Nevada, 2003.

Lamsal, L. N., Martin, R. V., Padmanabhan, A., van Donkelaar, A., Zhang, Q., Sioris, C. E., Chance, K., Kurosu, T. P., and Newchurch, M. J.: Application of satellite observations for timely updates to global anthropogenic NO_x emission inventories, Geophys. Res. Lett., 38, L05810, doi:10.1029/2010GL046476, 2011.

Lapina, K., Henze, D. K., Milford, J. B., Huang, M., Lin, M., Fiore, A. M., Carmichael, G., Pfister, G. G., and Bowman, K.: Assessment of source contributions to seasonal vegetative exposure to ozone in the U.S., J. Geophys. Res.-Atmos., 119, 324–340, 2014.

Levelt, P. F., van den Oord, G. H. J., Dobber, M. R., Malkki, A., Visser, H., de Vries, J., Stammes, P., Lundell, J. O. V., and Saari, H.: The Ozone Monitoring Instrument, IEEE T. Geosci. Remote, 44, 1093–1101, 2006.

Liang, Q., Jaegle, L., Jaffe, D. A., Weiss-Penzias, P., Heckman, A., and Snow, J. A.: Long-range transport of Asian pollution to the northeast Pacific: seasonal variations and transport pathways of carbon monoxide, J. Geophys. Res., 109, D23S07, doi:10.1029/2003JD004402, 2004.

Liang, Q., Jaegle, L., and Wallace, J. M.: Meteorological indices for Asian outflow and transpacific transport on daily to interannual timescales, J. Geophys. Res., 110, D18308, doi:10.1029/2005JD005788, 2005.

Lin, J.-T.: Satellite constraint for emissions of nitrogen oxides from anthropogenic, lightning and soil sources over East China on a high-resolution grid, Atmos. Chem. Phys., 12, 2881–2898, doi:10.5194/acp-12-2881-2012, 2012.

Lin, J.-T. and McElroy, M. B.: Detection from space of a reduction in anthropogenic emissions of nitrogen oxides during the Chinese economic downturn, Atmos. Chem. Phys., 11, 8171–8188, doi:10.5194/acp-11-8171-2011, 2011.

Lin, J.-T., Wuebbles, D. J., and Liang, X. Z.: Effects of intercontinental transport on surface ozone over the United States: present and future assessment with a global model, Geophys. Res. Lett., 35, L02805, doi:10.1029/2007GL031415, 2008.

ACPD
14, 19515–19544, 2014

Lin, J.-T., Liu, Z., Zhang, Q., Liu, H., Mao, J., and Zhuang, G.: Modeling uncertainties for tropospheric nitrogen dioxide columns affecting satellite-based inverse modeling of nitrogen oxides emissions, Atmos. Chem. Phys., 12, 12255–12275, doi:10.5194/acp-12-12255-2012, 2012.

Lin, J.-T., Pan, D., Davis, S. J., Zhang, Q., He, K., Wang, C., Streets, D. G., Wuebbles, D. J., and Guan, D.: China's international trade and air pollution in the United States, P. Natl. Acad. Sci. USA, doi:10.1073/pnas.1312860111, 2014a.

Lin, J.-T., Martin, R. V., Boersma, K. F., Sneep, M., Stammes, P., Spurr, R., Wang, P., Van Roozendael, M., Clémer, K., and Irie, H.: Retrieving tropospheric nitrogen dioxide from the Ozone Monitoring Instrument: effects of aerosols, surface reflectance anisotropy, and vertical profile of nitrogen dioxide, Atmos. Chem. Phys., 14, 1441–1461, doi:10.5194/acp-14-1441-2014, 2014b.

Liu, J. and Mauzerall, D. L.: Estimating the average time for inter-continental transport of air pollutants, Geophys. Res. Lett., 32, L11814, doi:10.1029/2005GL022619, 2005.

Mao, J., Paulot, F., Jacob, D. J., Cohen, R. C., Crounse, J. D., Wennberg, P. O., Keller, C. A., Hudman, R. C., Barkley, M. P., and Horowitz, L. W.: Ozone and organic nitrates over the eastern United States: sensitivity to isoprene chemistry, J. Geophys. Res.-Atmos., 118, 11256–11268, doi:10.1002/jgrd.50817, 2013.

Mijling, B., van der A, R. J., and Zhang, Q.: Regional nitrogen oxides emission trends in East Asia observed from space, Atmos. Chem. Phys., 13, 12003–12012, doi:10.5194/acp-13-12003-2013, 2013.

Millet, D. B., Jacob, D. J., Boersma, K. F., Fu, T. M., Kurosu, T. P., Chance, K., Heald, C. L., and Guenther, A.: Spatial distribution of isoprene emissions from North America derived from formaldehyde column measurements by the OMI satellite sensor, J. Geophys. Res., 113, D02307, doi:10.1029/2007JD008950, 2008.

Olivier, J. G. J. and Berdowski, J. J. M.: Global emissions sources and sinks, in: The Climate System, edited by: Berdowski, J., Guicherit, R., and Heij, B. J., 33–78, A. A. Balkema Publishers/Swets & Zeitlinger Publishers, Lisse, the Netherlands, 2001a.

Parrington, M., Jones, D. B. A., Bowman, K. W., Horowitz, L. W., Thompson, A. M., Tarasick, D. W., and Witte, J. C.: Estimating the summertime tropospheric ozone distribution over North America through assimilation of observations from the Tropospheric Emission Spectrometer, J. Geophys. Res., 113, D18307, doi:10.1029/2007JD009341, 2008.

ACPD
14, 19515–19544, 2014

Parrington, M., Palmer, P. I., Henze, D. K., Tarasick, D. W., Hyer, E. J., Owen, R. C., Helmig, D., Clerbaux, C., Bowman, K. W., Deeter, M. N., Barratt, E. M., Coheur, P.-F., Hurtmans, D., Jiang, Z., George, M., and Worden, J. R.: The influence of boreal biomass burning emissions on the distribution of tropospheric ozone over North America and the North Atlantic during 2010, Atmos. Chem. Phys., 12, 2077–2098, doi:10.5194/acp-12-2077-2012, 2012.

Pechony, O., Shindell, D. T., and Faluvegi, G.: Direct top-down estimates of biomass burning CO emissions using TES and MOPITT versus bottom-up GFED inventory, J. Geophys. Res.-Atmos., 118, 8054–8066, doi:10.1002/jgrd.50624, 2013.

Shim, C., Wang, Y., Choi, Y., Palmer, P. I., Abbot, D. S., and Chance, K.: Constraining global isoprene emissions with Global Ozone Monitoring Experiment (GOME) formaldehyde column measurements, J. Geophys. Res., 110, D24301, doi:10.1029/2004JD005629, 2005.

Singh, K., Jardak, M., Sandu, A., Bowman, K., Lee, M., and Jones, D.: Construction of non-diagonal background error covariance matrices for global chemical data assimilation, Geosci. Model Dev., 4, 299–316, doi:10.5194/gmd-4-299-2011, 2011.

Valin, L. C., Russell, A. R., Hudman, R. C., and Cohen, R. C.: Effects of model resolution on the interpretation of satellite NO_2 observations, Atmos. Chem. Phys., 11, 11647–11655, doi:10.5194/acp-11-11647-2011, 2011.

van der Werf, G. R., Randerson, J. T., Giglio, L., Collatz, G. J., Mu, M., Kasibhatla, P. S., Morton, D. C., DeFries, R. S., Jin, Y., and van Leeuwen, T. T.: Global fire emissions and the contribution of deforestation, savanna, forest, agricultural, and peat fires (1997–2009), Atmos. Chem. Phys., 10, 11707–11735, doi:10.5194/acp-10-11707-2010, 2010.

Verstraeten, W. W., Boersma, K. F., Zörner, J., Allaart, M. A. F., Bowman, K. W., and Worden, J. R.: Validation of six years of TES tropospheric ozone retrievals with ozonesonde measurements: implications for spatial patterns and temporal stability in the bias, Atmos. Meas. Tech., 6, 1413–1423, doi:10.5194/amt-6-1413-2013, 2013.

Vestreng, V. and Klein, H.: Emission data reported to UNECE/EMEP, Quality assurance and trend analysis and Presentation of WebDab, Norwegian Meteorological Institute, Oslo, Norway, MSC-W Status Report, 2002.

Voulgarakis, A., Telford, P. J., Aghedo, A. M., Braesicke, P., Faluvegi, G., Abraham, N. L., Bowman, K. W., Pyle, J. A., and Shindell, D. T.: Global multi-year O_3–CO correlation patterns from models and TES satellite observations, Atmos. Chem. Phys., 11, 5819–5838, doi:10.5194/acp-11-5819-2011, 2011.

ACPD
14, 19515–19544, 2014

Walker, T. W., Martin, R. V., van Donkelaar, A., Leaitch, W. R., MacDonald, A. M., Anlauf, K. G., Cohen, R. C., Bertram, T. H., Huey, L. G., Avery, M. A., Weinheimer, A. J., Flocke, F. M., Tarasick, D. W., Thompson, A. M., Streets, D. G., and Liu, X.: Trans-Pacific transport of reactive nitrogen and ozone to Canada during spring, Atmos. Chem. Phys., 10, 8353–8372, doi:10.5194/acp-10-8353-2010, 2010.

Wang, Y., Konopka, P., Liu, Y., Chen, H., Müller, R., Plöger, F., Riese, M., Cai, Z., and Lü, D.: Tropospheric ozone trend over Beijing from 2002–2010: ozonesonde measurements and modeling analysis, Atmos. Chem. Phys., 12, 8389–8399, doi:10.5194/acp-12-8389-2012, 2012.

Wang, Y. X., McElroy, M. B., Jacob, D. J., and Yantosca, R. M.: A nested grid formulation for chemical transport over Asia: applications to CO, J. Geophys. Res., 109, D22307, doi:10.1029/2004JD005237, 2004.

Wild, O., Fiore, A. M., Shindell, D. T., Doherty, R. M., Collins, W. J., Dentener, F. J., Schultz, M. G., Gong, S., MacKenzie, I. A., Zeng, G., Hess, P., Duncan, B. N., Bergmann, D. J., Szopa, S., Jonson, J. E., Keating, T. J., and Zuber, A.: Modelling future changes in surface ozone: a parameterized approach, Atmos. Chem. Phys., 12, 2037–2054, doi:10.5194/acp-12-2037-2012, 2012.

Worden, H. M., Logan, J. A., Worden, J. R., Beer, R., Bowman, K., Clough, S. A., Eldering, A., Fisher, B. M., Gunson, M. R., Herman, R. L., Kulawik, S. S., Lampel, M. C., Luo, M., Megretskaia, I. A., Osterman, G. B., and Shephard, M. W.: Comparisons of Tropospheric Emission Spectrometer (TES) ozone profiles to ozonesondes: methods and initial results, J. Geophys. Res., 112, D03309, doi:10.1029/2006JD007258, 2007.

Worden, H. M., Deeter, M. N., Edwards, D. P., Gille, J. C., Drummond, J. R., and Nédélec, P.: Observations of near surface carbon monoxide from space using MOPITT multispectral retrievals, J. Geophys. Res., 115, D18314, doi:10.1029/2010JD014242, 2010.

Yan, Y.-Y., Lin, J.-T., Kuang, Y., Yang, D.-W., and Zhang, L.: Tropospheric carbon monoxide over the Pacific during HIPPO: two-way coupled simulation of GEOS-Chem and its multiple nested models, Atmos. Chem. Phys., submitted, 2014.

Zhang, L., Jacob, D. J., Bowman, K. W., Logan, J. A., Turquety, S., Hudman, R. C., Li, Q.-B., Beer, R., Worden, H. M., Worden, J. R., Rinsland, C. P., Kulawik, S. S., Lampel, M. C., Shephard, M. W., Fisher, B. M., Eldering, A., and Avery, M. A.: Ozone-CO correlations determined by the TES satellite instrument in continental outflow regions, Geophys. Res. Lett., 33, L18804, doi:10.1029/2006GL026399, 2006.

ACPD
14, 19515–19544, 2014

Zhang, L., Jacob, D. J., Boersma, K. F., Jaffe, D. A., Olson, J. R., Bowman, K. W., Worden, J. R., Thompson, A. M., Avery, M. A., Cohen, R. C., Dibb, J. E., Flock, F. M., Fuelberg, H. E., Huey, L. G., McMillan, W. W., Singh, H. B., and Weinheimer, A. J.: Transpacific transport of ozone pollution and the effect of recent Asian emission increases on air quality in North America: an integrated analysis using satellite, aircraft, ozonesonde, and surface observations, Atmos. Chem. Phys., 8, 6117–6136, doi:10.5194/acp-8-6117-2008, 2008.

Zhang, L., Jacob, D. J., Kopacz, M., Henze, D. K., Singh, K., and Jaffe, D. A.: Intercontinental source attribution of ozone pollution at western U.S. sites using an adjoint method, Geophys. Res. Lett., 36, L11810, doi:10.1029/2009GL037950, 2009a.

Zhang, Q., Streets, D. G., Carmichael, G. R., He, K. B., Huo, H., Kannari, A., Klimont, Z., Park, I. S., Reddy, S., Fu, J. S., Chen, D., Duan, L., Lei, Y., Wang, L. T., and Yao, Z. L.: Asian emissions in 2006 for the NASA INTEX-B mission, Atmos. Chem. Phys., 9, 5131–5153, doi:10.5194/acp-9-5131-2009, 2009b.

ACPD
14, 19515–19544, 2014

Table 1. Monthly regional mean O_3 and CO correlation and slope for the free troposphere (825–383 hPa) for June, July and August 2006–2010. The numbers of TES are black. The numbers of model are red in the parentheses. The model results are smoothed with the TES averaging kernels.

Region	Type	Month	2006	2007	2008	2009	2010	MEAN
Eastern China	dO_3/dCO	Jun	0.36 (0.25)	0.17 (−0.06)	0.19 (0.14)	0.14 (0.02)	0.18 (0.29)	0.22 (0.25)
		Jul	0.08 (0.38)	0.29 (0.36)	0.23 (0.34)	0.15 (0.44)	0.38 (0.19)	
		Aug	0.20 (0.27)	0.22 (0.26)	0.32 (0.20)	0.15 (0.18)	0.29 (0.47)	
	R	Jun	0.66 (0.39)	0.47 (−0.11)	0.45 (0.30)	0.51 (0.10)	0.70 (0.52)	0.50 (0.37)
		Jul	0.23 (0.61)	0.66 (0.57)	0.49 (0.38)	0.50 (0.57)	0.53 (0.24)	
		Aug	0.33 (0.38)	0.52 (0.43)	0.54 (0.28)	0.39 (0.22)	0.56 (0.64)	
China Outflow	dO_3/dCO	Jun	0.32 (0.60)	0.49 (0.43)	0.52 (0.62)	0.59 (0.66)	0.64 (0.76)	0.55 (0.70)
		Jul	0.56 (0.59)	0.50 (0.48)	0.65 (0.83)	0.63 (1.05)	0.75 (1.13)	
		Aug	0.55 (0.85)	0.32 (0.49)	0.51 (0.61)	0.53 (0.51)	0.67 (0.89)	
	R	Jun	0.69 (0.57)	0.71 (0.41)	0.76 (0.62)	0.68 (0.35)	0.73 (0.55)	0.67 (0.57)
		Jul	0.73 (0.57)	0.66 (0.47)	0.66 (0.69)	0.59 (0.70)	0.73 (0.78)	
		Aug	0.68 (0.71)	0.55 (0.46)	0.63 (0.60)	0.58 (0.39)	0.74 (0.75)	

ACPD
14, 19515–19544, 2014

Table 2. Regional total contributions of anthropogenic and lightning NO_x on free tropospheric (819–396 hPa) O_3 over eastern China and the China Outflow region. The value can be explained as the percentage change of regional mean O_3 (Eastern China, China Outflow) due to 100 % increase of NO_x in a particular region (China and ROA). The regions of China and ROA are defined in Fig. 3. The perturbation values (Pt) are the relative difference between standard and perturbation simulations.

Type		Eastern China				China Outflow			
		DJF	MAM	JJA	SON	DJF	MAM	JJA	SON
NO_x Anthro	China	2.68 %	5.17 %	10.16 %	7.08 %	2.62 %	5.24 %	8.27 %	5.76 %
	China (Pt)	2.85 %	5.29 %	10.12 %	6.91 %	2.90 %	5.46 %	8.16 %	5.68 %
	ROA	1.72 %	2.04 %	2.28 %	2.00 %	2.17 %	2.42 %	3.49 %	2.97 %
NO_x lightning	China	0.18 %	1.64 %	6.39 %	1.47 %	0.31 %	2.31 %	6.54 %	1.71 %
	ROA	0.81 %	2.18 %	2.63 %	1.99 %	1.16 %	3.11 %	4.03 %	2.90 %

ACPD
14, 19515–19544, 2014

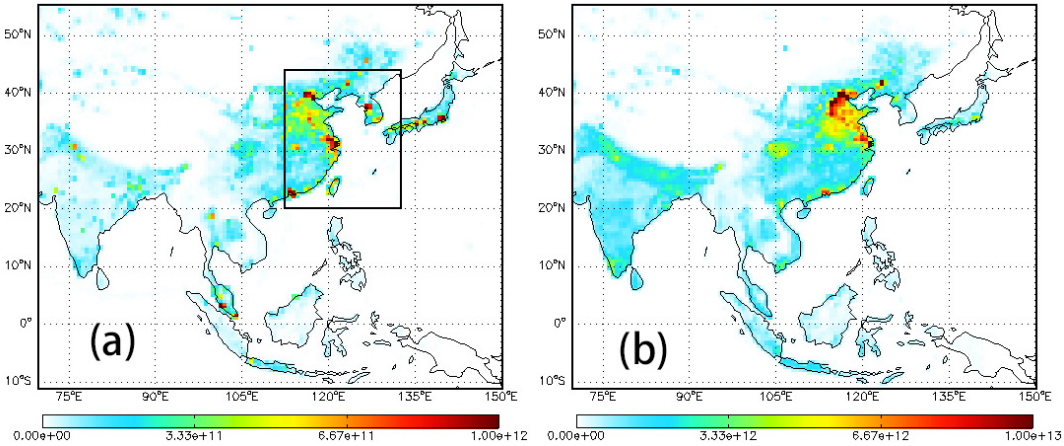

Figure 1. Anthropogenic emission of **(a)** NO_x and **(b)** CO in June 2006 as used in GEOS-Chem. The unit is molec cm^{-2} s^{-1}. The black box defines the domains studied in this work. The "East China" domain includes the grids of Chinese mainland within the black box. The "China Outflow region" are grids within the black box, excluding the Chinese mainland.

ACPD
14, 19515–19544, 2014

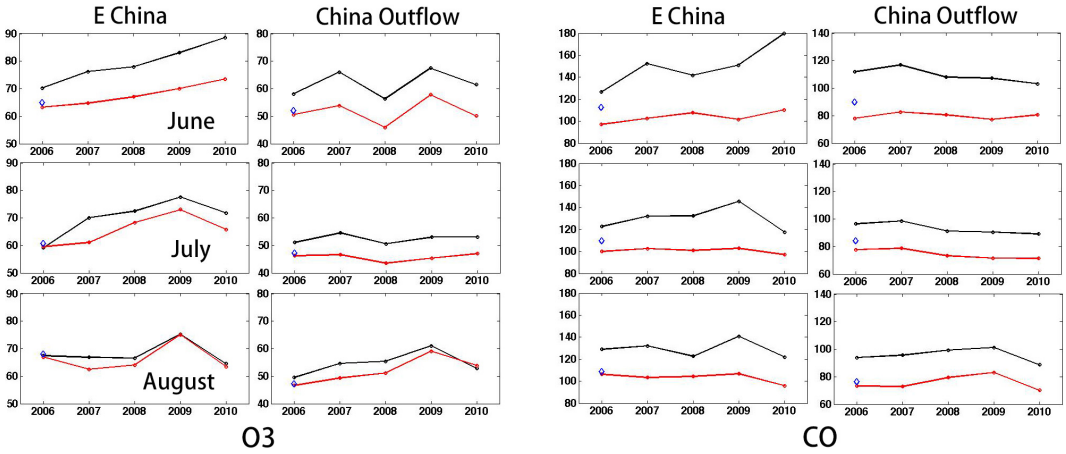

Figure 2. Monthly regional mean O_3 and CO concentration at 681 hPa in June, July and August 2006–2010. Red line is GEOS-Chem model simulation with a priori emission inventories and black line is TES measurements. The blue diamonds show the a posteriori model simulation in 2006 with updated NO_x and CO inventories. The posterior model results are smoothed wth the TES averaging kernels. The TES ozone data are biased high by 7 ppbv.

ACPD
14, 19515–19544, 2014

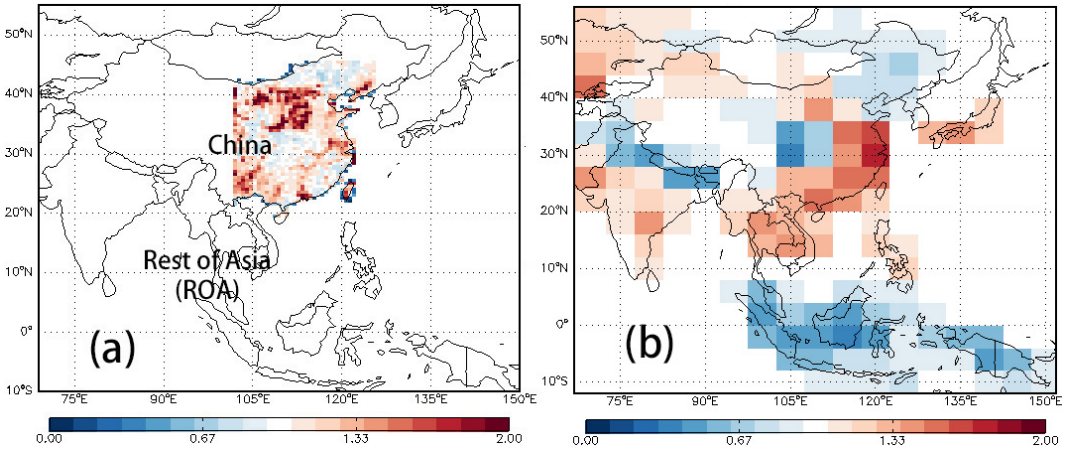

Figure 3. (a) Scaling factors of anthropogenic NO_x for June 2006. **(b)** Scaling factor of total CO emission (combustion + oxidation from biogenic VOCs) for June 2006.

ACPD
14, 19515–19544, 2014

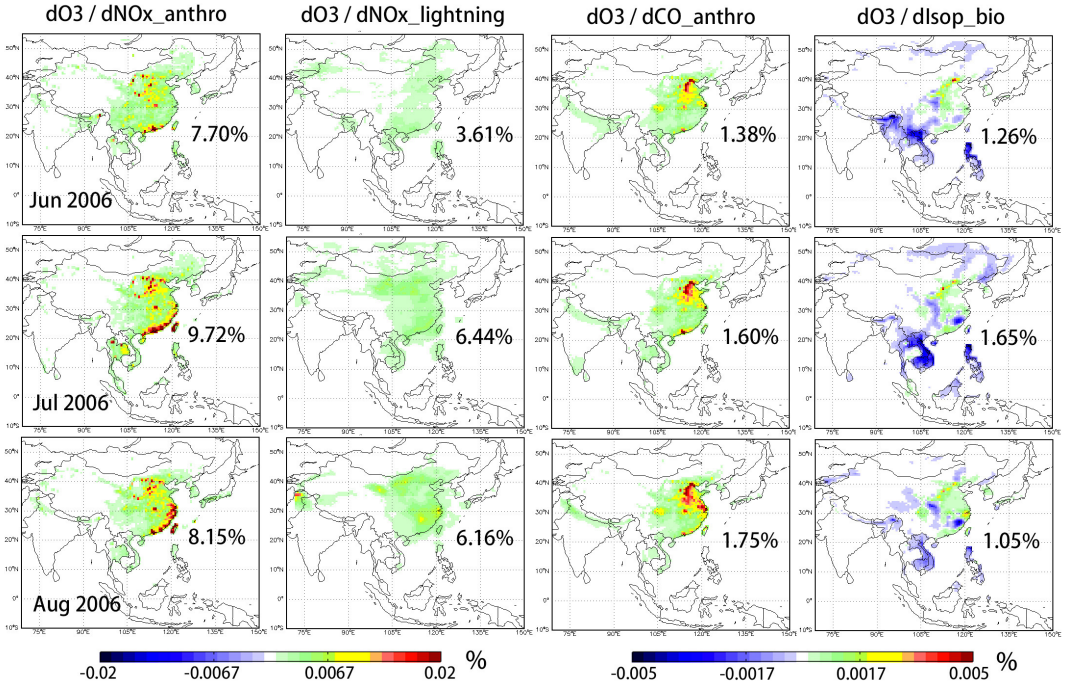

Figure 4. Contributions of anthropogenic NO_x, lightning NO_x, anthropogenic CO, biogenic isoprene on free tropospheric (819–396 hPa) O_3 over eastern China derived from the adjoint of GEOS-Chem. The contributions can be explained as the percentage change of regional mean ozone due to a fractional change in the emissions in a particular grid assuming unchanged chemical environment. The numbers are the total of absolute value of pre-cursor contributions for the whole domain shown in the figures.

ACPD
14, 19515–19544, 2014

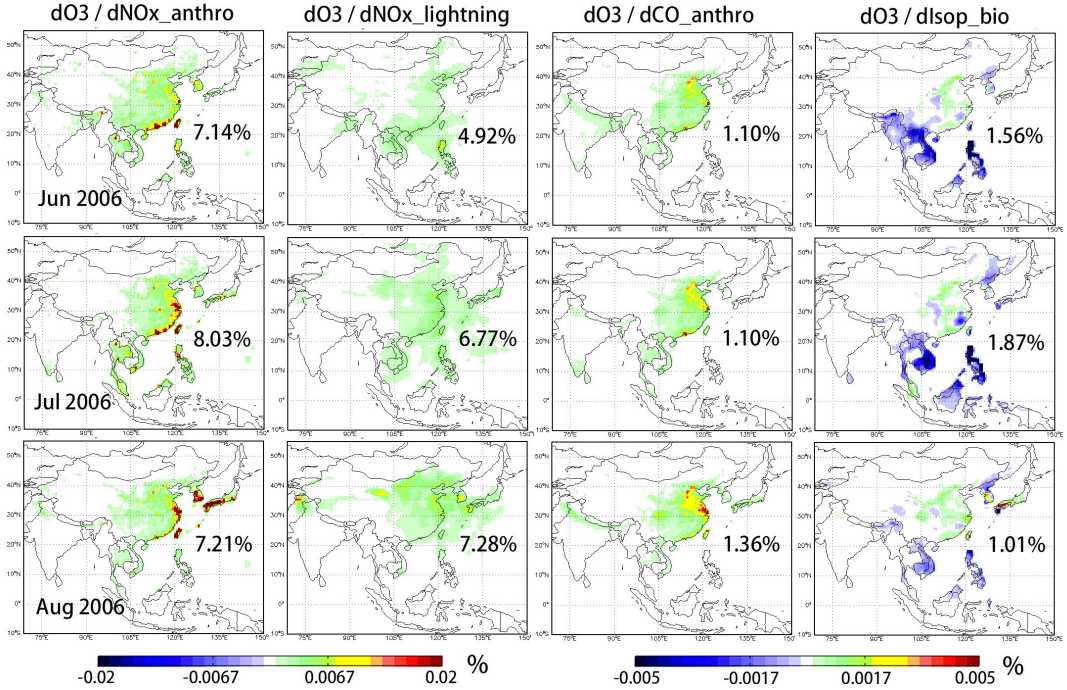

Figure 5. Contributions of anthropogenic NO_x, lightning NO_x, anthropogenic CO, biogenic isoprene on free tropospheric (819–396 hPa) O_3 over China Outflow region derived from the adjoint of GEOS-Chem.

ACPD
14, 19515–19544, 2014

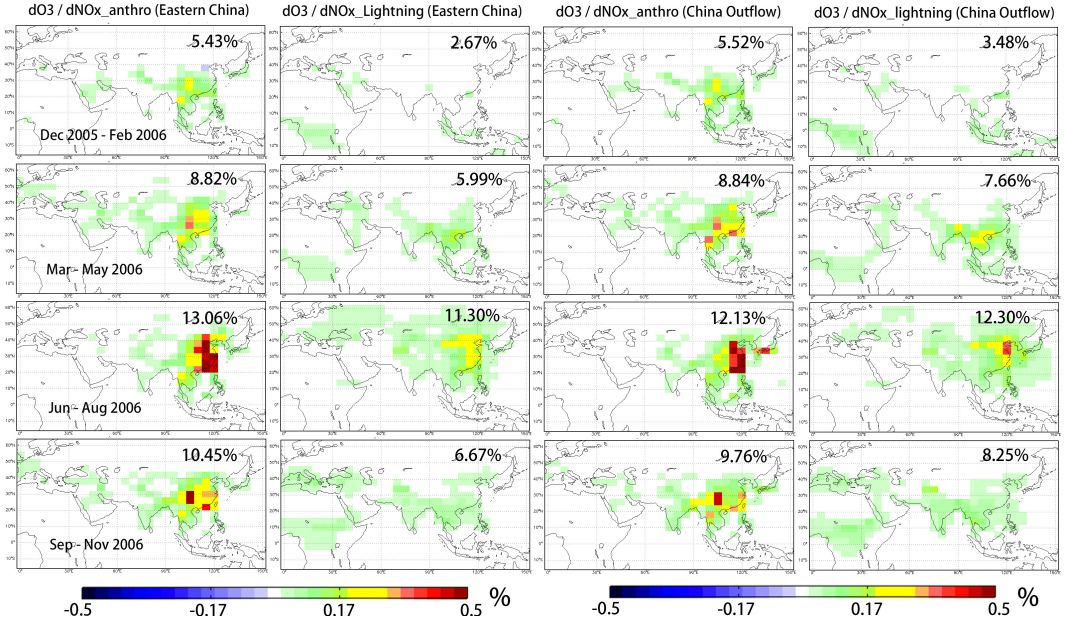

Figure 6. Contributions of anthropogenic NO_x and lightning NO_x on free tropospheric (819–396 hPa) O_3 over eastern China and China outflow region.

ACPD
14, 19515–19544, 2014